Hindawi Publishing Corporation
Journal of Materials
Volume 2013, Article ID 393017, 6 pages
http://dx.doi.org/10.1155/2013/393017

Research Article

Parameter Optimization in the Synthesis of BZT Ceramics to Achieve Good Dielectric Properties

A. Frattini,[1,2] A. Di Loreto,[1,2] and O. De Sanctis[2]

[1] *Área Física, Departamento de Química-Física, FCByF, UNR, Suipacha 531, 2000 Rosario, Argentina*
[2] *Laboratorio de Materiales Cerámicos, FCEIyA, IFIR, UNR, Pellegrini 250, 2000 Rosario, Argentina*

Correspondence should be addressed to A. Di Loreto; diloreto@fceia.unr.edu.ar

Received 14 November 2012; Revised 16 March 2013; Accepted 18 March 2013

Academic Editor: Antoni Morawski

The powder synthesis of barium zirconate titanate (BZT) ($BaZr_xTi_{(1-x)}O_3$) from the mechanochemical activation of $BaCO_3$, ZrO_2, and TiO_2 was studied. The grinding effect, by using a planetary ball milling, on the crystallization temperature of BZT powders ($x = 0.05$) was analyzed. X-ray diffractometry, differential thermal analysis, thermogravimetric analysis, and scanning electronic microscopy (SEM) were used as characterization methods. The crystallization behavior of powders activated by high-energy grinding and the effect of grinding time on the BZT crystallization were analyzed. After grinding by 4 h, the $BaZr_{(0.05)}Ti_{(0.95)}O_3$ sample was almost fully crystallized at 800°C. The results of dielectric and ferroelectric properties show that high-energy ball milling is a practical and promising way to prepare BZT ceramics.

1. Introduction

Ferroelectric materials based in Pb have been studied for many years for its important applications in piezoelectric, pyroelectric, and optical devices [1–5]. Lead-free compositions can be of great interest for environmentally friendly applications such as actuators and dielectrics for capacitors. $BaTiO_3$ is the most widely used ferroelectric material in ceramic capacitors and is known for its large electrochemical coupling factor [2, 3]. Within $BaTiO_3$ family, barium zirconate titanate ($Ba(Zr_xTi_{(1-x)})O_3$, BZT) has become one of the most attractive materials because it has been reported that the zirconium substitutions into the titanium lattices enhance the dielectric and piezoelectric properties [6, 7]. Furthermore, Curie temperature can be shifted below room temperature by doping with Zr [8, 9]. However, under common preparation conditions, BZT ceramics have very high sintering temperature that does not fit the industrial requirements. In order to decrease the sintering temperature, it is necessary to produce powders with fine particle sizes and homogeneous distribution.

Mechanochemical activation by mixing of high energy (high-energy ball milling) has become important to produce solid-state reactions at lower temperatures than those used in conventional methods of powder preparation [10–14]. This mechanical technique is unique because of its advantages: (i) low cost of starting materials, (ii) low operating temperature, and (iii) higher sinterability of milled powders.

The purpose of this work is to reach low energy cost in the synthesis of BZT ceramics without expense of their electrical properties. The effects of increasing the milling time of the powders and, on the other hand, of lowering the powder calcination temperature and/or sintering temperature of the pellets are analyzed.

2. Experimental

BZT ceramics were prepared via conventionally mixed-oxide method by high-energy ball milling. Commercial powders of barium carbonate ($BaCO_3$) (99.98% Sigma-Aldrich), titanium dioxide (TiO_2) (99.98% Sigma-Aldrich), and zirconium oxide (ZrO_2) (99.9% Sigma-Aldrich), were used as starting materials with the nominal composition of $BaZr_{0.05}Ti_{0.95}O_3$. The precursors were ground in a planetary ball milling (Torrey Hills Technologies ND 0.4L) during 1, 2, and 4 h,

into a zirconia jars. Simultaneous differential thermal analysis (DTA) and thermogravimetric analysis (TGA) measurements were carried out on the as-obtained powder from 20°C to 1200°C at 10°C/min heating rate, with 50 mL/min of O_2 flux into alumina crucibles, using a Shimadzu DTG-60 analyzer. The mixed powders were calcined between 600°C and 1200°C for 2 h in the air. Afterwards, powders were analyzed by X-ray diffraction (XRD-Philips PW1700 diffractometer), scanning electron microscopy (SEM Philips 505), and high-resolution SEM (FEI QUANTA 200).

The powders with two weight percent PVB binder were uniaxially pressed (200 MPa) into green pellets with 10 mm of diameter and 1 mm of thickness. The sintering behavior of these pellets was monitored at constant heating rate (5°C/min) in a Theta Dilatronic dilatometer. Structural analyses of sintered samples at 1350°C and 1400°C were performed by XRD and SEM.

To measure the electric properties, the surfaces were polished, and silver electrodes were painted on both sides of the pellets. The capacitance and dielectric loss of the samples were measured with a HP 4192A impedance analyzer, and the hysteresis loops were examined by using a conventional Sawyer-Tower tester at 50 Hz.

3. Results and Discussion

Figures 1 and 2 show the DTA-TGA curves of the oxides mixture milled for 1 and 4 h, respectively, when they were heated from room temperature to 1200°C. Three endothermic peaks (labeled as (1), (2), and (3)) are observed in both DTA curves. The first two peaks match with weight losses, whereas no weight loss is seen for the last one. It is well known [15, 16] that the first two peaks correspond to reactions of $BaCO_3$ decomposition and synthesis of $BaTiO_3$, including the formation of a transient Ba_2TiO_4 phase. These reactions are as follows:

$$BaCO_3 + TiO_2 \longrightarrow BaTiO_3 + CO_2 \quad (1)$$

where the CO_2 emission causes the first weight loss realized in the TGA graph (around 600°C),

$$BaCO_3 + BaTiO_3 \longrightarrow Ba_2TiO_4 + CO_2 \quad (2)$$

where again there is weight loss by the CO_2 emission, and

$$Ba_2TiO_4 + TiO_2 \longrightarrow 2BaTiO_3 \quad (3)$$

which has no weight loss associated.

By comparing both figures, it is noted that the peak (1) is broader and deeper in Figure 2 which means further development of reaction (1) in the sample milled by 4 h and matches with the greater mass loss (about double) observed in the TGA curve. This behavior also agrees with the smaller depth of peak (2) in Figure 2 since more $BaCO_3$ has decomposed and also with the 800°C XRD patterns in Figures 3(a) and 3(b), where it is quite clear that there is fewer remaining $BaCO_3$ in the sample milled for 4 h.

It is noteworthy that the formation of Ba_2TiO_4 phase advances at the temperature range between 600°C and 900°C

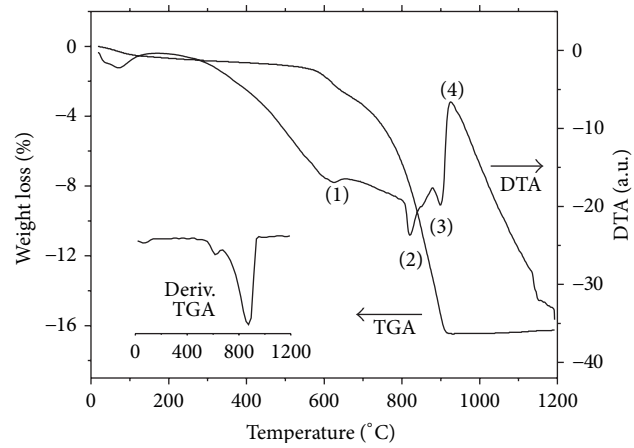

Figure 1: DTA-TG of BZT powder milled for 1 h (10°C/min heating rate, sample weight = 30.158 mg).

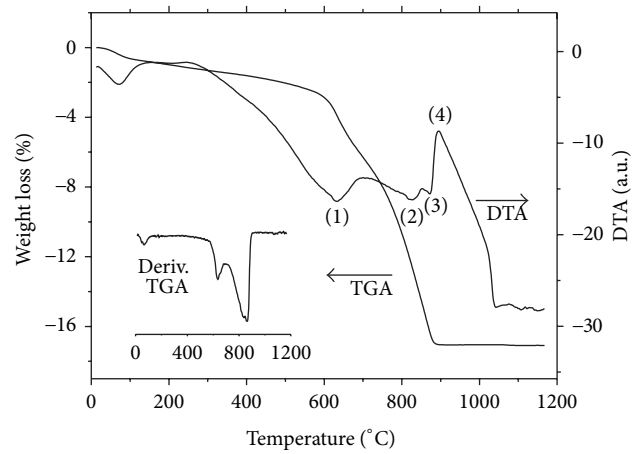

Figure 2: DTA-TG of BZT powder milled for 4 h (10°C/min heating rate, sample weight = 28.135 mg).

due to the diffusive nature of this reaction [15]. The peak (2) in Figure 1 is quite sharp since superposes the $\gamma \rightarrow \beta$ allotropic transition of $BaCO_3$ (at 827°C) [17] with reaction (2). As it is observed, this peak in Figure 2 is not so deep because that transition is hindered by the lattice deformation resulting of the greater milling time.

On the other hand, Figure 2 shows an increase in the mass loss rate (see the derivative of the TGA curve from the inset) because of the higher reactivity of the powders and the faster kinetic of the reaction. Furthermore, the mass loss finishes at 885°C in the BZT-4 h sample and at 920°C for the BZT-1 h one. By revising DTA graphs, only reaction (3) could be present from these temperatures until the maximum of hump (4). This temperature defines the synthesis of $BaTiO_3$ after accomplishment of all the reactions above mentioned.

Berbenni et al. [18] have obtained a final plateau in its TG curve at 730°C by applying high-energy milling for 159 h on BZT powders. By analyzing the temperatures where the mass loss is over, Berbenni's results and ours indicate that crystallization starts at lower temperatures if more energy

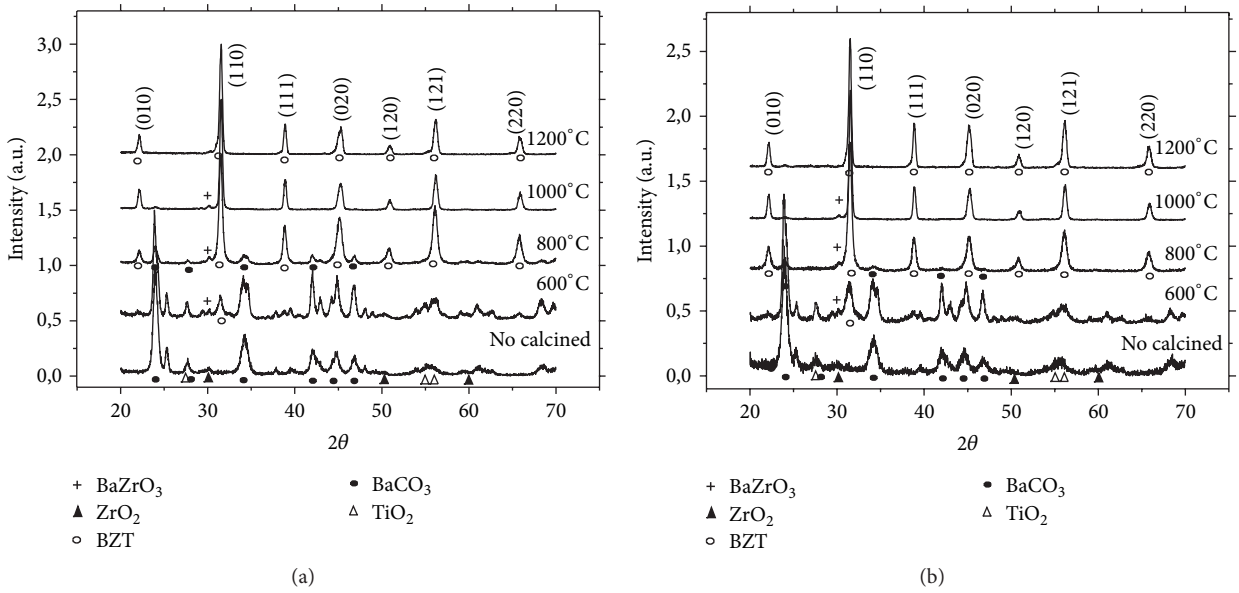

Figure 3: (a) XRD of 1 h milled powders as calcination temperature function. (b) XRD of 4 h milled powders as calcination temperature function.

from milling is delivered. That is to say, by increasing the milling time the powders will have more reactivity because of their smaller particle size and hence higher surface area. By comparing the end of hump (4) in both DTA curves, it is clear that the sample ground for 4 h has completely crystallized at 1040°C. The sample milled for 1 h seems to be completely crystallized at 1200°C. Finally, from Figures 1 and 2, it can be expected that Ba_2TiO_4 and BZT coexist only in samples calcined in temperatures ranging between 700°C and 900°C.

XRD patterns of both samples (Figures 3(a) and 3(b)) are on good agreement with the DT and TG analysis. The diffractogram of 600°C for the 4 h milled sample shows the main peak of BZT sharper and higher than the one corresponding to the 1 h milled sample. The 800°C pattern for the 1 h ground sample (Figure 3(a)) shows clear presence of $BaCO_3$ peaks yet (23.89°, 27.71°, 34.08°, 34.58°, 41.98°, 42.95°, and 46.77°) while they have disappeared in the 4 h ground sample (Figure 3(b)).

Furthermore, in the 800°C-4 h ground XRD pattern (Figure 3(b)), the BZT seems to be practically crystallized; just some peaks of $BaCO_3$ and the strongest of cubic $BaZrO_3$ ($2\theta = 30.14°$) are weakly seen. At 1000°C, there only remains the main peak of $BaZrO_3$, whereas, at 1200°C, the sample is fully crystallized. Even though the DTA and TGA graphics have suggested possible presence of Ba_2TiO_4 phase between 800°C and 900°C, this phase has not been detected in the XRD patterns. It is worth noting that XRD measurements were carried out on samples previously calcined for 2 h, while thermal measurements have a quite different thermal evolution (10°C/min). The calcination for 2 h could have increased the Ba_2TiO_4 diffusion, and there it will be transformed completely into $BaTiO_3$ [15].

Figure 4 shows the milling time effect on powders calcined at 1200°C for 2 h. The peaks are broad, showing poorly crystallized phases with amorphous phases for unmilled

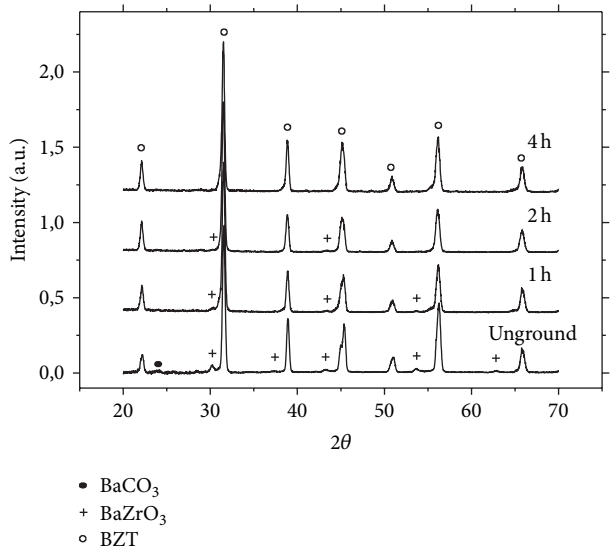

Figure 4: XRD of BZT powders milled during different times and calcined at 1200°C for 2 h.

powders. They become stronger and sharper when the samples are milled. It is observed that the unground sample presents peaks corresponding to $BaCO_3$ ($2\theta = 24.09°$) and $BaZrO_3$ ($2\theta = 30.14°$, 37.14°, 43.14°, 53.54°, and 62.67°). After grinding by 1 hour, the samples did not exhibit $BaCO_3$, but, however, the $BaZrO_3$ content decreased gradually as the milling time increased. Finally, a BZT structure free of spurious phases was obtained after 4 h of grinding and 2 h of calcination at 1200°C. The crystallite sizes of powders calcined at different times were calculated from the X-ray broadening of (110) peaks, using the Scherrer equation [19]. Crystallite sizes for powders treated at 1 h, 2 h, and 4 h are 32.9, 33.8, and

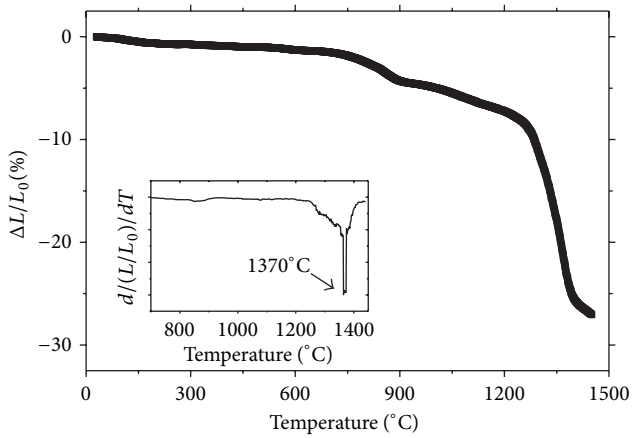

Figure 5: Linear shrinkage and linear shrinkage rate (inset) as a temperature function. The pellets were fabricated from powder calcined at 800°C.

35.7 nm, respectively. This indicates that BZT crystallizes and grows as the milling time increases.

The curves of linear shrinkage and its derivative with respect to temperature ($d(\Delta L/L_0)/dT$), both as functions of temperature, are shown in Figure 5. The first contraction between 750°C and 900°C indicates powder agglomeration during the sintering due to processes inside the agglomerates and between them [20]. Densification then increases sharply (~20%) in the range from 1250°C up to 1400°C. From these data, the 1350°C and 1400°C values were set as suitable temperatures for the sintering of ceramic pellets.

The SEM from Figure 6(a) indicates that the average grain size of ceramic is 250 nm, which means that grains have not grown in the sintering process with respect to the initial size of the crystallites in the powders (Figure 6(b)). However, certain porosity can be seen in the micrograph presumably induced by a binder evaporation and/or by a residual inhomogeneity in the shape of the calcined crystallites. Indeed, if the calcined crystallites are irregularly shaped prior to pressing, greater porosity will result in the sintered ceramic.

Figure 7 shows the XRD patterns of BZT pellets sintered at 1350°C and 1400°C. BZT pellets sintered at 1400°C display full crystallization in a perovskite phase, while small peaks of secondary phase are noted in the sample sintered at 1350°C. Moreover, larger grain growth is detected in the 1400°C sample. Precisely for both ceramics, crystallite sizes of 56.3 nm and 58.9 nm were calculated from half-width of (011) peaks.

The sintering temperature has significant influence on the electrical properties as displayed in Figure 8. The behavior of the dielectric constant (ε_r) with frequency [1 kHz–1 MHz] is similar in both samples (1350°C and 1400°C), but their values are higher, in all this range, for the sample sintered at 1400°C. The comparison between both samples in the range 1 kHz–10 kHz is reported at the inset. Furthermore, the dielectric loss (D) in both samples decreases with the increasing frequency in this range, this value being lower for the sample sintered at 1400°C. These two behaviors come from a further densification at higher temperature.

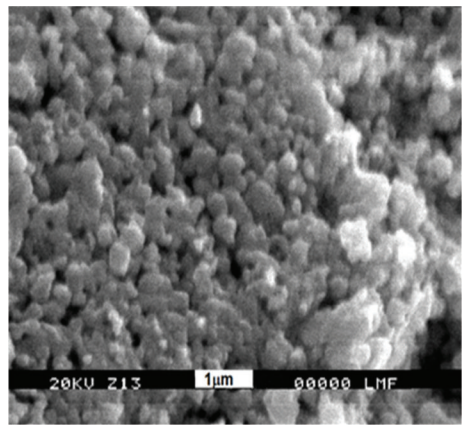

(a)

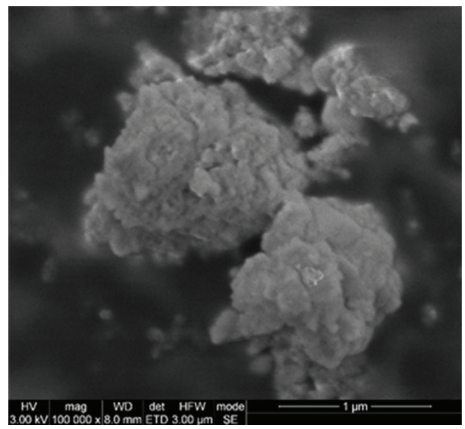

(b)

Figure 6: (a) SEM of the ceramic sintered at 1350°C. (b) HRSEM of ground powders by 4 h.

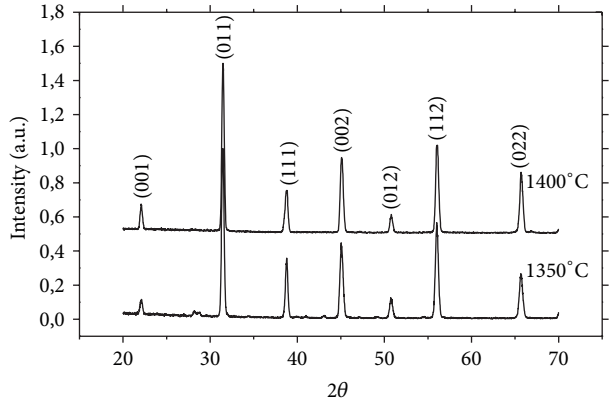

Figure 7: XRD of BZT pellets sintered at 1350°C and 1400°C.

Figure 9(a) shows the dielectric constant evolution of the BZT sample (sintered at 1400°C) with the temperature, where the three curves correspond to measurements at 10, 50, and 100 kHz. The ceramic presents two abrupt changes in dielectric constant corresponding to the orthorhombic-tetragonal (~60°C) and tetragonal-cubic (~125°C) phase transitions, displaying a typical ferroelectric behavior [21–23].

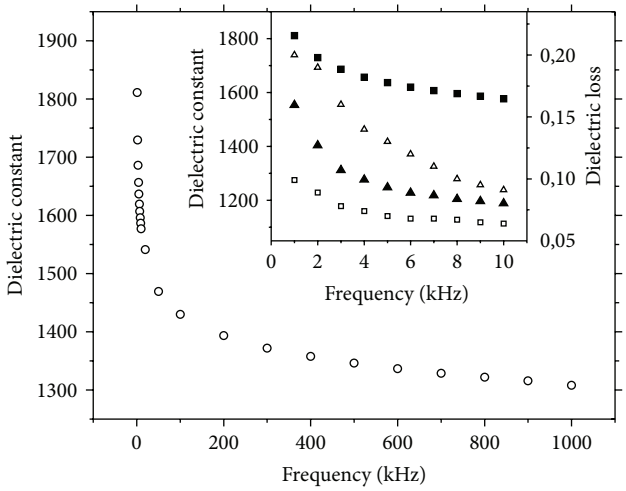

Figure 8: Dielectric constant (ε_r) of BZT sintered at 1400°C. Inset: zoom for {1–10 kHz} range, Δ: ε_r for sample sintered at 1400°C, ▲: ε_r for 1350°C sintered BZT, □: dielectric loss for 1350°C sintered BZT, ■: dielectric loss for 1400°C sintered BZT.

Besides, it is not observed a T_C shift (Curie temperature) with frequency, according to a nonrelaxor ferroelectric.

The Curie temperature increases slightly as does the sintering temperature; it can be seen in Figure 9(b). Moreover, the orthorhombic to tetragonal transition phase around 60°C is more evident in the sample sintered at 1400°C.

The hysteresis cycle measured at 50 Hz and room temperature, with the sample inside of silicon oil, is shown in Figure 10. Typical performances of normal ferroelectrics, according to the designed ceramic composition, were observed. The sample sintered at 1400°C shows a remnant polarization of 35 μC/cm^2 and a coercive electric field of about 2.5 kV/cm, while the 1350°C sintered ceramic shows lower values in its ferroelectric properties.

These results can be compared to the dielectric constant and the ferroelectric P-E hysteresis loops previously reported. Nanakorn et al. [23] have obtained 25 μC/cm^2 for remnant polarization and about 3000 as dielectric constant (ε_r) in ceramics of BZT ($x = 0.05$). Their procedure involved ball milling in acetone during 24 h, calcination at 1200°C for 2 h, milling for 24 h in ethanol, and sintering at 1300°C–1450°C for 2 h. Similar method has been used by Yu et al. [24] (except for sintering at 1500°C–1560°C from 2 to 15 h) and they have found values of 13.3 μC/cm^2 and $\varepsilon_r = 1600$ for $BaZr_{(0.05)}Ti_{(0.95)}O_3$ ceramics.

4. Conclusions

The purpose of reaching low energy cost in the synthesis of BZT ceramics was achieved. By high-energy milling, suitable crystallization of $BaZr_{0.05}Ti_{0.95}O_3$ powders was achieved at 800°C due to the increasing in their reactivity. From these powders, BZT ceramics were sintered for 2 h at 1350°C and 1400°C. BZT ceramics with high values of remnant polarization (35 μC/cm^2) and good values of dielectric constant (1700

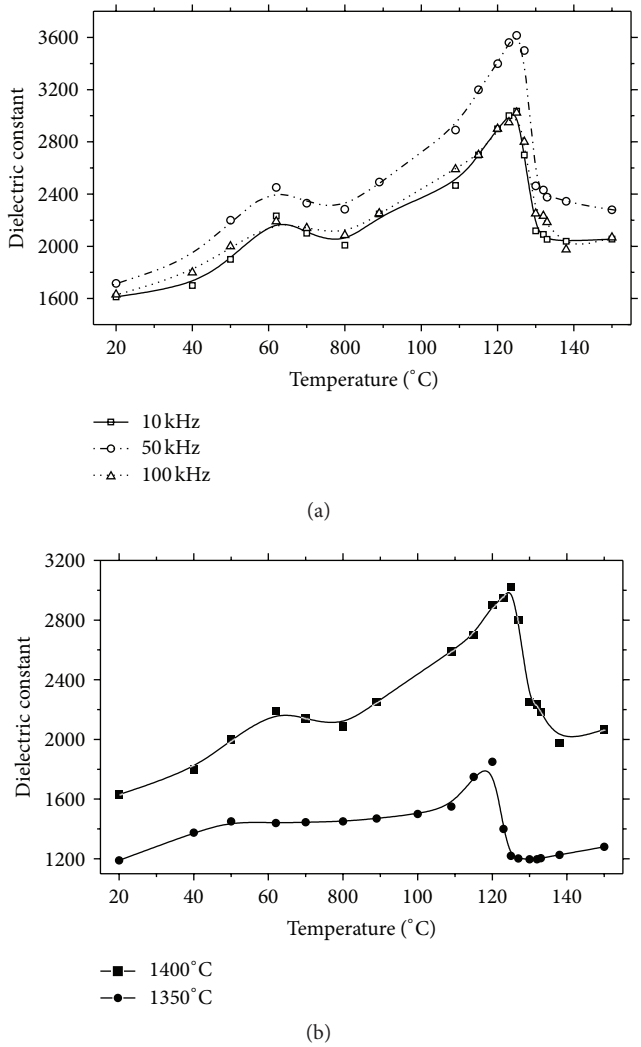

Figure 9: (a) Dielectric constant versus temperature and frequency for the sample sintered at 1400°C, measured at room temperature. (b) Dielectric constant versus temperature for ceramics sintered at 1350°C and 1400°C, measured at 100 kHz and room temperature.

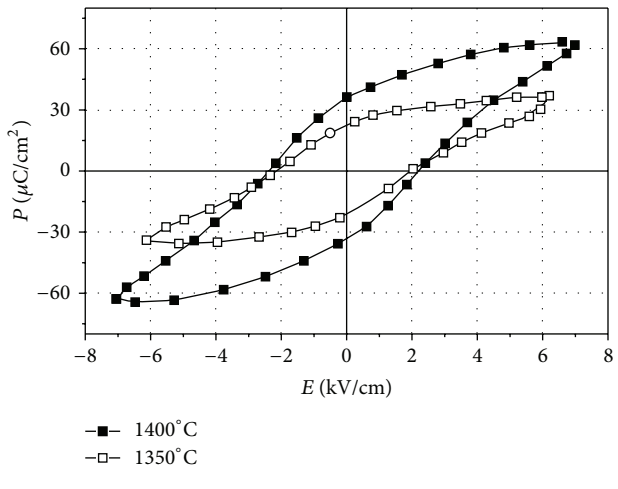

Figure 10: Polarization versus electric field for BZT sintered at 1400°C, measured at 50 Hz and room temperature.

at room temperature) were obtained. These results show an efficient way in the synthesis of BZT ceramics as compared to other proceedings reported in the literature.

Moreover, several common features of these ceramics were found in our samples, summarized as follows. The dielectric constant drops when the frequency rises at the range from 1 kHz to 1 MHz. The Curie temperature does not change with frequency but grows slightly with sintering temperature increasing. Furthermore, sintering at 1400°C improves the dielectric properties (rise of ε and decreasing of D) with regard to sintering at 1350°C.

References

[1] Y. Xu, *Ferroelectric Materials and Their Applications*, North Holland, 1991.

[2] M. T. Sebastian, *Dielectric Materials for Wireless Comunications*, Elsevier, 2008.

[3] R. Frank, *Understanding Smart Sensors*, Artech House, 2000.

[4] B. Jaffe, W. R. Cook, and H. Jaffe, *Piezoelectric Ceramics*, Academic Press, 1971.

[5] A. Moulson and J. Herbert, *Electroceramics: Materials-Properties-Applications*, John Wiley & Sons, 2003.

[6] U. Weber, G. Greuel, U. Boettger, S. Weber, D. Hennings, and R. Waser, "Dielectric properties of $Ba(Zr,Ti)O_3$-based ferroelectrics for capacitor applications," *Journal of the American Ceramic Society*, vol. 84, pp. 759–766, 2001.

[7] K.-i. Mimura, T. Naka, T. Shimura, W. Sakamoto, and T. Yogo, "Synthesis and dielectric properties of $(Ba,Ca)(Zr,Ti)O_3$ thin films using metal-organic precursor solutions," *Thin Solid Films*, vol. 516, no. 23, pp. 8408–8413, 2008.

[8] A. Simon, J. Ravez, and M. Maglione, "Relaxor properties of $Ba_{0.9}Bi_{0.067}(Ti_{1-x}Zr_x)O_3$ ceramics," *Solid State Sciences*, vol. 7, no. 8, pp. 925–930, 2005.

[9] S. Lee, M. Kwak, S. Moon, H. Ryu, Y. Kim, and K. Kang, *Integrated Ferroelectrics*, vol. 77, pp. 93–99, 2005.

[10] C. Suryanarayana, *Progress in Materials Science*, vol. 46, pp. 1–184, 2001.

[11] J. Lee, M. Choi, N. Hung et al., *Ceramics International*, vol. 33, pp. 1283–1286, 2007.

[12] R. Rajkhowa, L. Wang, and X. Wang, "Ultra-fine silk powder preparation through rotary and ball milling," *Powder Technology*, vol. 185, no. 1, pp. 87–95, 2008.

[13] C. B. Reid, J. S. Forrester, H. J. Goodshaw, E. H. Kisi, and G. J. Suaning, "A study in the mechanical milling of alumina powder," *Ceramics International*, vol. 34, no. 6, pp. 1551–1556, 2008.

[14] C. Gomez-Yañez, C. Benitez, and H. Balmori-Ramirez, "Mechanical activation of the synthesis reaction of $BaTiO_3$ from a mixture of $BaCO_3$ and TiO_2 powders," *Ceramics International*, vol. 26, no. 3, pp. 271–277, 2000.

[15] A. Beauger, J. C. Mutin, and J. C. Niepce, "Synthesis reaction of metatitanate $BaTiO_3$—part 1 Effect of the gaseous atmosphere upon the thermal evolution of the system $BaCO_3$-TiO_2," *Journal of Materials Science*, vol. 18, no. 10, pp. 3041–3046, 1983.

[16] L. B. Kong, J. Ma, H. Huang, R. F. Zhang, and W. X. Que, "Barium titanate derived from mechanochemically activated powders," *Journal of Alloys and Compounds*, vol. 337, no. 1-2, pp. 226–230, 2002.

[17] L. Templeton and J. Pask, "Formation of $BaTiO_3$ from $BaCO_3$ and TiO_2 in air and in CO_2," *Journal of the American Ceramic Society*, vol. 42, pp. 212–216, 1959.

[18] V. Berbenni, A. Marini, and G. Bruni, "Effect of mechanical milling on solid state formation of $BaTiO_3$ from $BaCO_3$-TiO_2 (rutile) mixtures," *Thermochimica Acta*, vol. 374, no. 2, pp. 151–158, 2001.

[19] A. West, *Solid State Chemistry and Its Applications*, John Wiley & Sons, 1992.

[20] F. Moura, A. Z. Simões, B. D. Stojanovic, M. A. Zaghete, E. Longo, and J. A. Varela, "Dielectric and ferroelectric characteristics of barium zirconate titanate ceramics prepared from mixed oxide method," *Journal of Alloys and Compounds*, vol. 462, no. 1-2, pp. 129–134, 2008.

[21] A. Ioachim, M. I. Toacsan, M. G. Banciu et al., "Synthesis and properties of $Ba(Zn_{1/3}Ta_{2/3})O_3$ for microwave and millimeter wave applications," *Thin Solid Films*, vol. 516, no. 7, pp. 1558–1562, 2008.

[22] T. Maiti, R. Guo, and A. S. Bhalla, "Structure-property phase diagram of $BaZr_xTi_{1-x}O_3$ system," *Journal of the American Ceramic Society*, vol. 91, no. 6, pp. 1769–1780, 2008.

[23] N. Nanakorn, P. Jalupoom, N. Vaneesorn, and A. Thanaboonsombut, "Dielectric and ferroelectric properties of $Ba(Zr_xTi_{1-x})O_3$ ceramics," *Ceramics International*, vol. 34, no. 4, pp. 779–782, 2008.

[24] Z. Yu, C. Ang, R. Guo, and A. S. Bhalla, "Piezoelectric and strain properties of $Ba(Ti_{1-x}Zr_x)O_3$ ceramics," *Journal of Applied Physics*, vol. 92, no. 3, 1489.